Parametric excitation of magnetic vortex gyrations in spin-torque nano-oscillators

P. Bortolotti,[1,*] E. Grimaldi,[1,2] A. Dussaux,[1,†] J. Grollier,[1] V. Cros,[1] C. Serpico,[3] K. Yakushiji,[4] A. Fukushima,[4] H. Kubota,[4] R. Matsumoto,[4] and S. Yuasa[4]

[1]*Unité Mixte de Physique CNRS/Thales and Université Paris Sud 11, 1 avenue Fresnel, 91767 Palaiseau, France*

[2]*CNES, 18 av. Edouard Belin, 31400 Toulouse, France*

[3]*Dipartimento di Ingegneria Elettrica e Tecnologie dell'Informazione, Universitá di Napoli Federico II, Via Claudio 21, Napoli, Italy*

[4]*Institute of Advanced Industrial Science and Technology (AIST), Spintronics Research Center, Tsukuba, Japan*

(Received 1 March 2013; revised manuscript received 10 September 2013; published 20 November 2013)

We experimentally demonstrate that large amplitude magnetic vortex gyrations can be parametrically excited by the injection of radio-frequency (rf) current at twice the natural frequency of the gyrotropic vortex-core motion. The mechanism of excitation is based on the *parallel pumping* of vortex motion by the rf orthoradial field generated by the injected current. Theoretical analysis shows that experimental results can be interpreted as the manifestation of *parametric amplification* when the rf current is small, and of *parametric instability* when the rf current is above a certain threshold. By taking into account the energy nonlinearities, we succeed to describe the amplitude saturation of vortex oscillations as well as the coexistence of stable regimes.

DOI: 10.1103/PhysRevB.88.174417 PACS number(s): 75.47.−m, 75.40.Gb, 85.30.Mn, 85.75.−d

I. INTRODUCTION

Parametric excitations and parametric resonance are long-known phenomena in classical physics.[1] They occur in systems with periodically varying parameters and may result in large excitations by appropriately tuning the frequency of parametric changes with the natural frequency of the system.[2] The most common example of a parametrically excited system is a person on a swing, the dynamics of which can be analyzed as a pendulum with varying length.[3] The swing dynamics is archetypal to parametric phenomena present in many systems of interest in mechanical, civil, and naval engineering.[4] In addition, the possibility to use parametric phenomena to improve the sensitivity of microelectromechanical systems (MEMS) is recently under intense investigation.[5,6]

In the area of electrical and telecommunication engineering, parametric amplification was actively studied before the advent of the transistor, as a technique to obtain low-noise amplifiers,[7] and it is recently receiving renewed interest.[8] The principle of operation of the parametric amplifier can be clearly illustrated in reference to *LC*-based electronic oscillators. The time-varying parameter is usually the junction capacitance of a reverse biased diode and the capacitance is controlled by the voltage across the junction. The parametric pumping is obtained by increasing the capacitance when the capacitor is charged and decreasing it when the capacitor is discharged. A net gain is obtained when the frequency f of the parametric variations satisfies the conditions $f \approx 2f_0/n$, where f_0 is the natural frequency of the oscillator of the system and n a positive integer.

In applied magnetism, the parametric excitations of magnetization oscillations have been extensively studied in the area of ferromagnetic resonance[9] in connection with the processes of spin-wave instability[10] and parallel pumping.[11] These phenomena are driven by the modulation of the oscillation frequency of elementary excitations (spin waves) associated with the spatially uniform magnetic ground state obtained by a strong bias field. In the case of spin-wave instability, the spatially uniform mode is driven to a large precession angle by radio-frequency (rf) fields applied transversal to the bias field. The modulation of the spin-wave spectrum is due to the nonlinear coupling of the uniform precession with spin waves. On the other hand, in the case of parallel pumping, the rf field is applied along the direction of the bias field, and thus directly modulates the frequency of spin-wave modes.[11]

In this paper, we investigate the implementation of the principle of *parallel pumping* in spin-torque devices having a vortex in the free magnetic layer both experimentally and theoretically. It is an unconventional case of parallel pumping because the field used to modulate the frequency of magnetization oscillations is the orthoradial magnetic field generated by the injected current (usually referred to as the Oersted field). The frequency of this modulation is chosen to be twice the frequency of the lowest frequency mode present in a magnetic thin disk with a vortex ground state, which is the translational motion of the vortex core.[12]

The present investigation is relevant to the development and control of spintronics rf oscillators in large excitation regimes.[13] These oscillators promise to have an important role in forthcoming microwave communication technologies.[14,15] A striking result in this area has been the development of spin-torque nano-oscillators (STNOs), tunable over a wide frequency range by the injected current both for uniform[16–18] and nonuniform[19–21] magnetic configurations. The performances of these devices in terms of power and linewidth have been constantly improved over the past few years.[22–28] In particular, it has been recently demonstrated[29–31] that magnetic tunnel junction (MTJ) pillars with a vortex ground state[32–34] allow one to obtain a signal with a large output power ($\simeq$1 μW) and very good coherence ($\simeq$1 MHz). It is crucial to gain an understanding of the dynamics of these oscillators in regimes where the vortex is driven very far from the equilibrium position, as is the case in the present study.

Parametric resonance by means of parallel pumping in a spin-valve nanopillar has been previously studied by Urazhdin *et al.*[35] in the more traditional setting where the magnetic free layer is uniformly magnetized and the pumping rf field,

generated by an antenna, is applied along the spatially uniform bias field. In addition, the somehow related phenomenon of phase locking of spin-torque auto-oscillations by an external source at double frequency has been investigated both in the case of a uniformly magnetized free layer,[35] and in the case of a vortex state free layer.[36,37]

Here, we study parametric excitations of a vortex MTJ subject to an external rf current with a frequency close to $2f_0$, where f_0 is the gyrotropic resonance frequency of the vortex core with a dc current below the threshold for self-oscillations (subcritical case). The use of the dc current in our experiments is aimed to obtain a partial compensation of dissipative damping effects by means of the spin-torque effect. In order to have sufficient efficiency in the damping compensation, a large enough out-of-plane component of the magnetization in the polarizing layer is required, and this is realized by applying a strong out-of-plane static field. This field leads to an out-of-plane component of the vortex curling in the free layer which is, for this reason, in the vortex core state.[12] The lowest frequency magnetization dynamic mode in the free layer is the gyrotropic motion of the vortex core, which is mainly determined by a confining potential due to magnetostatic and current produced fields. The parallel pumping is realized by modulating the gyrotropic frequency of the vortex through the rf variations of the Oersted field. The resulting gyrotropic motion exhibits two specific features of parametric resonance of weakly dissipative oscillators. The first effect, usually referred to as *parametric amplification* (see, e.g., *Rugar et al.*[5]), consists in the amplification of signals which contain the frequencies close to the natural oscillation frequency of the vortex. In our case, it manifests itself in the amplification of the thermally activated vortex motion around its equilibrium position. The second effect is the *parametric instability* that takes place when the power of the rf excitation exceeds a certain threshold at which both the amplitude and the coherence of the oscillations strongly increase. Eventually saturation is reached due to nonlinearities. An interesting feature of the steady state reached after the instability is the *coexistence* of the large parametrically excited regime with the static equilibrium point (thermally excited vortex resonance). This coexistence, and the related hysteresis phenomena, are predicted by the theory in the absence of thermal fluctuations. In the experiments at room temperature, this feature manifests itself in the thermal hopping of the system between the two stable regimes and it is detected by the presence of doubly peaked power spectra.

In the following, we will first present the experimental results of parametric excitation. Then we will show how we can describe the evolution of the magnetization with our analytical model, and finally we will compare the analytical and the experimental results.

II. EXPERIMENTS

A. Methods

We perform our measurements on several circular MTJs of radius $R = 250$ nm. The complete structure (with thickness in nm) is PtMn (15)/CoFe (2.5)/Ru (0.85)/CoFeB (3)/MgO (1.075)/NiFe (5)/Ta (7)/Ru (6)/Cr (5)/Au (200). The 5-nm-thick NiFe free layer presents a vortex magnetization at remanence. The resistance-area (RA) product is $\simeq 8.8\ \Omega\,\mu\text{m}^2$. The MTJ resistance at the saturated parallel state is $R_P \simeq 45\ \Omega$ with an average magnetoresistance $\Delta R \simeq 8.5\ \Omega$ at room temperature. The measurement circuit is described in Fig. 1. The sample is subjected to a magnetic field, which can be applied at any angle compared to the plane of the sample. Both a dc and an rf current are applied perpendicular to the plane of the sample [current-perpendicular-to-plane (CPP) geometry]. A spectrum analyzer and a nanovoltmeter are connected in parallel in order to control both the rf and dc components of the output signal. The dc and rf parts of the circuit are separated through a bias tee. Two dc blocks prevent extra dc current to reach the rf instruments and an attenuator is added to minimize the noise in the measurement. A typical measurement consists of the following steps: (i) Apply the external field H_{ext}. (ii) Apply the dc current I_{dc}. (iii) Apply the rf current I_{rf} at a frequency sufficiently far from the frequency of interest, i.e., $f_{\text{rf}} \ll 2f_0$ or $f_{\text{rf}} \gg 2f_0$. (iv) Sweep the frequency of the rf current f_{rf} in the desired frequency range.

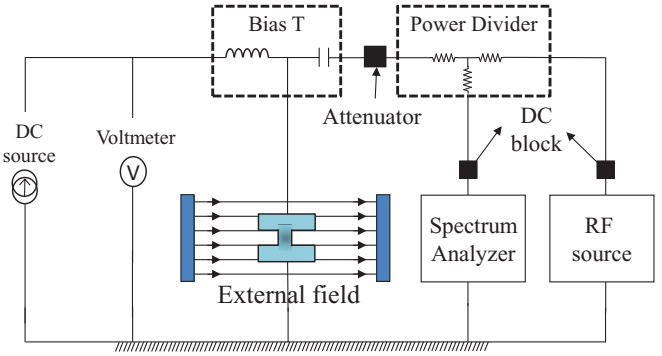

FIG. 1. (Color online) Scheme of the circuit used in the experiments.

For all of the presented measurements, the field is applied out of plane with an amplitude of $H_{\text{ext},z} = 4.48$ kG. In our convention, a positive current means electrons flowing from the free layer to the SyntheticAntiFerromagnet (SAF) stack. We emphasize that the injected dc current I_{dc} is always below the threshold I_{th} necessary to excite large amplitude vortex-core sustained oscillations, which, depending on the sample, can vary between $4 < I_{\text{th}} < 5$ mA. Consequently, when no I_{rf} current is applied, the small I_{dc} induces only small fluctuations of the vortex core around its equilibrium position and a very weak signal is measured at $f_0 \simeq 140$ MHz with a maximum fitted power of about 3 nW/GHz/mA^2 and a large linewidth (about 12 MHz). These figures are typical of thermal-induced vortex-core oscillations.[29,38,39]

B. Results

The main features of the microwave signal are modified when an additional current I_{rf} is injected at a frequency close to $2f_0$. In Fig. 2(a), we first present the color-scale map of the power spectral density (PSD) as a function of the frequency of the current $I_{\text{rf}} = 0.8$ mA (rms value) corresponding to an rf power of -18 dBm. A signal emerges from the background level when $264 < f_{\text{rf}} < 278$ MHz, which corresponds to a fre-

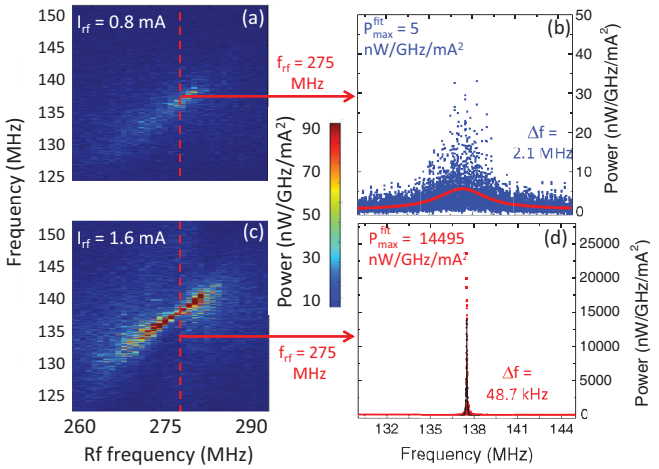

FIG. 2. (Color online) (a)–(c) Colored maps of emitted power for the frequency of the gyrotropic core motion vs the external rf frequency measured (a) for a small $I_{rf} = 0.8$ mA (corresponding to a power of -18 dBm) and (c) a large $I_{rf} = 1.6$ mA (corresponding to -12 dBm) current (rms value). $I_{dc} = 3$ mA and $H_{perp} = 4.48$ kG. Both currents and field are applied perpendicular to the sample plane. (b)–(d) Power spectral density vs frequency measured with an external rf current at $f_{rf} = 275$ MHz.

quency around twice the natural frequency f_0 of the system. As shown in Fig. 2(b), the spectrum measured for $f_{rf} = 275$ MHz can be fitted by a Lorentzian distribution. A maximum fitted power of 5 nW/GHz/mA^2, twice as large as the thermal one, is observed. The corresponding linewidth is also reduced by one order of magnitude to 2.1 MHz compared to the case with $I_{rf} = 0$ mA. These measurements are a clear example of *parametric amplification* of the vortex dynamics in the regime of subcritical I_{dc} currents and are consistent with the ones presented by Urazhdin *et al.*[35] for the case of uniform magnetization under a parametric rf field.

The situation changes drastically when $I_{rf} > 1$ mA. We enter into a new regime, i.e., the *parametric instability* regime, and a tremendous improvement in both the coherence and the emitted power is obtained. A striking example of such behavior is displayed in Fig. 2(c) for a large value of rf current, i.e., $I_{rf} = 1.6$ mA, corresponding to an rf power of -12 dBm. We find a large window of f_{rf}, i.e., between 265 and 285 MHz, in which the emitted power associated with the vortex dynamics comes out from the background level and the spectral linewidth reduces significantly. In this range, the vortex frequency increases linearly with f_{rf} and is strictly equal to $f_{rf}/2$. To demonstrate the drastic improvement of the rf features in this specific regime, we plot in Fig. 2(d) the peak detected for $f_{rf} = 275$ MHz. The maximum fitted power reaches 15 μW/GHz/mA^2 that is more than three orders of magnitude larger than the case of low rf power. The measured linewidth Δf of 49 kHz is indeed limited by the resolution bandwidth (RBW) of the spectrum analyzer (see the circuit scheme in Fig. 1) needed for measuring a large range of frequencies. Additional measurements with an optimized RBW allow us to extract a bottom limit value for the linewidth equal to 9 kHz.

III. VORTEX DYNAMICS: ANALYTICAL MODEL

It is assumed that the magnetization distribution in the disk-shaped free layer of the MTJ under investigation is determined by the position $\boldsymbol{X}$ of the vortex core both in static and dynamic conditions. A magnetization dynamics equation can be accordingly reduced to a Thiele-like equation[33] governing the dynamics of the variable $\boldsymbol{X}$. This equation, by making appropriate manipulations (see Appendix A for the details), can be reduced to the following form:

$$\frac{d\boldsymbol{x}}{dt} = \Omega(x,\jmath)\boldsymbol{e}_z \times \boldsymbol{x} - [d\Omega(x,\jmath) - c_z p_z \jmath]\,\boldsymbol{x} + \boldsymbol{v}, \qquad (1)$$

where $\boldsymbol{x} = \boldsymbol{X}/R$ is the vortex displacement measured in units of the pillar radius R, $x = |\boldsymbol{x}|$, and $\boldsymbol{e}_z$ is the z-axis unit vector directed perpendicular to the layers and oriented from the fixed layer to the free layer. The function $\Omega(x,\jmath)$ is the frequency of the vortex free gyrotropic oscillation as a function of x and the injected current density $\jmath$. It is given by the following expression:

$$\Omega(x,\jmath) = \Omega_{ms}\left[\frac{1}{1-(x/2)^2}\right] + \jmath\,\nu_{oe}\left(1 - \frac{x^2}{2}\right), \qquad (2)$$

where Ω_{ms} and ν_{oe} are two positive parameters taking into account the strength of the confining potential due to magnetostatic and Oersted fields, respectively [see Eqs. (B7) and (B8) for the exact form of Ω_{ms} and ν_{oe}]. The second term on the right-hand side (RHS) of Eq. (1) describes nonconservative contributions. In this term, the dimensionless parameter d is the normalized damping [see Eq. (B2)], the parameter c_z is the normalized spin-torque efficiency measured in units of frequency over current density [see Eq. (B4)], and $p_z = \cos\theta_p$, where θ_p is the angle that the polarizer magnetization forms with the z axis. The product $c_z p_z \jmath$ controls the intensity of the antidamping compensation due to the transfer of the spin angular momentum from the polarizer to the free layer.[29] Finally, the constant vector $\boldsymbol{v}$ is related to the effective in-plane field $\boldsymbol{H}_{\mathrm{eff},xy}$ acting on the vortex [see the discussion in Appendix A after Eq. (A8)].

The external excitations are taken into account by the terms $\jmath$ and $\boldsymbol{v}$. More specifically, we assume that the system is subject to a constant dc field and to a combination of dc and rf currents. This leads to the following decomposition of $\jmath$ and $\boldsymbol{v}$:

$$\jmath(t) = \jmath_{dc} + \jmath_{rf}\cos\omega_{rf}t, \qquad (3)$$

$$\boldsymbol{v}(t) = \boldsymbol{v}_{dc} + \boldsymbol{v}_{rf}\cos\omega_{rf}t. \qquad (4)$$

In the following we will analytically study Eq. (1) under the above time-varying excitation conditions (3) and (4) in order to find the parametric instability region for such a system (see Fig. 3).

We start our analysis by considering the stability of vortex small oscillations around the vortex-core static equilibrium position $\boldsymbol{x}_0 = \boldsymbol{X}_0/R$, which is established when only constant excitations are present, i.e., when $\jmath = \jmath_{dc}$. The equilibrium position can be computed by the following equation:

$$\Omega(x_0,\jmath_{dc})\boldsymbol{e}_z \times \boldsymbol{x}_0 + [c_z \jmath_{dc}\, p_z - d\,\Omega(x_0,\jmath_{dc})]\,\boldsymbol{x}_0 + \boldsymbol{v}_{dc} = 0, \qquad (5)$$

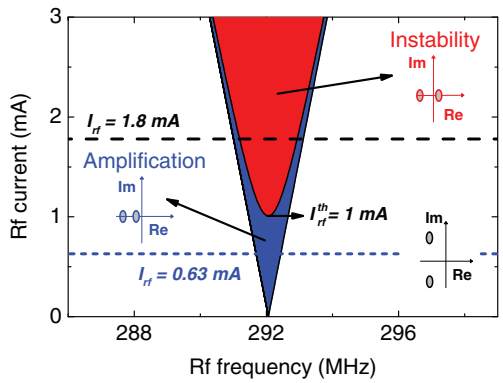

FIG. 3. (Color online) Phase diagram in the $(f_{\rm rf}, J_{\rm rf})$ plane with indications of the region of parametric instability (red) and parametric amplification (blue). Dashed lines represent two specific cases for $I_{\rm rf} = 1.8$ mA (−11 dBm) and $I_{\rm rf} = 0.6$ mA (−20 dBm). The values of the parameters used are $P = 0.225$, $I_{dc} = 2.5$ mA, $\alpha = 0.01$ (LL damping), and $x_0 = 0.3$.

where the term $\boldsymbol{v}_{\rm dc}$ [for the exact form observe that $\boldsymbol{v}_{\rm dc} = -\boldsymbol{e}_z \times \boldsymbol{f}_{\rm dc}$ and $\boldsymbol{f}_{\rm dc}$ is given by Eq. (B3) when $j = J_{\rm dc}$] is due to the effective in-plane field $\boldsymbol{H}_{{\rm eff},xy}$, which is assumed to be a few tens of Oersted. In these conditions $x_0 = |\boldsymbol{x}_0|$ is in the range $[0.1; 0.3]$.

By considering the expansion of Eq. (1) in terms of displacement from the equilibrium $\delta\boldsymbol{x} = \boldsymbol{x} - \boldsymbol{x}_0$, we obtain a differential equation for $\delta\boldsymbol{x}$ in the following form:

$$\frac{d}{dt}\delta\boldsymbol{x} = A_0(t)\cdot\delta\boldsymbol{x} + \boldsymbol{N}(t,\delta\boldsymbol{x}) + \boldsymbol{v}_{\rm rf}\cos\omega_{\rm rf}t, \tag{6}$$

where $\boldsymbol{N}(t,\delta\boldsymbol{x})$ contains all nonlinear terms in $\delta\boldsymbol{x}$. By choosing the x axis of the Cartesian reference in the direction of $\boldsymbol{x}_0$, the matrix $A_0(t)$ can be written as

$$A_0(t) = \begin{pmatrix} -d\widetilde{\omega}_1(t) + c_z p_z J(t) & -\widetilde{\omega}_2(t) \\ \widetilde{\omega}_1(t) & -d\widetilde{\omega}_2(t) + c_z p_z J(t) \end{pmatrix}, \tag{7}$$

where the two angular frequencies are given by

$$\widetilde{\omega}_1(t) = \Omega[x_0, j(t)] + x_0\frac{\partial}{\partial x_0}\Omega[x_0, j(t)], \tag{8a}$$

$$\widetilde{\omega}_2(t) = \Omega[x_0, j(t)]. \tag{8b}$$

By using Eq. (2) one obtains that

$$x_0\frac{\partial}{\partial x_0}\Omega[x_0, j(t)] \approx (\Omega_{\rm ms}/2 - \nu_{oe}J)x_0^2, \tag{9}$$

where we have neglected terms of fourth and higher order in x_0. From the above equations one can readily verify that the quantities appearing in the matrix A_0, i.e., Eq. (7), are given by the following expressions:

$$\widetilde{\omega}_{1,2}(t) = \omega_{1,2}[1 + q_{1,2}J_{\rm rf}\cos(2\pi f_{\rm rf}t)], \tag{10}$$

where

$$\omega_1 = \Omega(x_0, J_{\rm dc}) + (\Omega_{ms}/2 - \nu_{\rm oe}J_{\rm dc})x_0^2, \tag{11a}$$

$$\omega_2 = \Omega(x_0, J_{\rm dc}). \tag{11b}$$

The parameters q_1 and q_2, which are related to the rf component of the Oersted field confining potential, are given by

$$q_1 = \nu_{\rm oe}\left[1 - 3/2x_0^2\right]\omega_1, \tag{12a}$$

$$q_2 = \nu_{\rm oe}\left[1 - 1/2x_0^2\right]\omega_2. \tag{12b}$$

It is important to notice that conservative terms on the RHS of Eq. (6) are expected to be the dominant terms in vortex-core oscillations. The other terms act as perturbations. This fact can be used to discuss the parametric nature of the instability of small motion of the vortex core around $\boldsymbol{x}_0$.

To be more specific, let us write the linear equation obtained by Eq. (6) when the term $N(t,\delta\boldsymbol{x})$ is neglected. In addition, due to the fact that damping, rf excitations, and spin-torque terms are small perturbations of vortex dynamics, we can neglect in the diagonal elements of the matrix $A_0(t)$ all terms which are second order with respect to the quantities d, $J_{\rm rf}$, and $c_z p_z$. This leads to the equation

$$\begin{aligned}\frac{d}{dt}\delta\boldsymbol{x} = &\begin{pmatrix} -d\omega_1 + c_z p_z J_{\rm dc} & -\omega_2 \\ \omega_1 & -d\omega_2 + c_z p_z J_{\rm dc} \end{pmatrix}\cdot\delta\boldsymbol{x} \\ &+ J_{\rm rf}\cos(2\pi f_{\rm rf}t)\begin{pmatrix} 0 & -q_2\omega_2 \\ q_2\omega_2 & 0 \end{pmatrix}\cdot\delta\boldsymbol{x} \\ &+ \boldsymbol{v}_{\rm rf}\cos(2\pi f_{\rm rf}t),\end{aligned} \tag{13}$$

where the quantities $d\omega_{1,2} - c_z p_z J_{\rm dc}$, which control the damping of vortex-core small oscillations, are assumed to be both negative, as we assume that the dc current is below the threshold for self-oscillations. The solution of Eq. (13) is given by

$$\delta\boldsymbol{x} = \delta\boldsymbol{x}_h(t) + \delta\boldsymbol{x}_{\rm rf}(t), \tag{14}$$

where $\delta\boldsymbol{x}_h(t)$ and $\delta\boldsymbol{x}_{\rm rf}(t)$ are, respectively, the general solution of the homogeneous equation and the solution of the nonhomogeneous equation. The dominant terms in Eq. (13) are the time-independent off-diagonal terms of the first matrix on the RHS of the equation. If we neglect all other terms, the resulting vortex dynamics is free oscillations at the frequency $f_0 = \sqrt{\omega_1\omega_2}/(2\pi)$. As we are interested in studying excitations with $f_{\rm rf} \approx 2f_0$, it is expected that the solution $\delta\boldsymbol{x}_{\rm rf}(t)$ is small as it is driven by the off-resonance forcing term $\boldsymbol{v}_{\rm rf}\cos(2\pi f_{\rm rf}t)$. The term $\delta\boldsymbol{x}_h(t)$ is, on the other hand, a solution of a time-periodic homogenous linear equation [obtained by removing the term $\boldsymbol{v}_{\rm rf}\cos(2\pi f_{\rm rf}t)$ on the RHS of Eq. (13)] which has the usual form of a linear parametrically excited dynamical system.[3] For sufficiently large rf excitation, $\delta\boldsymbol{x}_h(t)$ may exponentially grow.

Before proceeding to a more detailed analysis of the instability, let us discuss briefly the physical origin of this process. The fact is that in general $\widetilde{\omega}_1(t) \neq \widetilde{\omega}_2(t)$ is a consequence of the break of the symmetry due to the in-plane field $\boldsymbol{H}_{{\rm eff},xy}$, and it is indeed this break that controls the coupling between vortex oscillations and parametric excitations. The situation is similar to the case of usual parallel pumping in rotationally symmetric systems. In that case, the coupling between the $2f_0$ excitations and the magnetization oscillations is controlled by the ellipticity of the amplitude which is due to the dipolar fields generated by the spin waves.[11] In our case instead, parametric pumping of vortex dynamics takes place only if $q_1 \neq q_2$, which occurs when the vortex oscillates around a displaced position.

To treat analytically Eq. (6), we first observe that the perturbative nature of the nonconservative terms on the RHS induces only slow changes of the vortex oscillation amplitude and phase. As a consequence, in order to describe this slow variation when $\omega_{\rm rf} \approx 2\omega_0$, it is convenient to make the following (Van Der Pol type) change of variable $\delta \boldsymbol{x} \mapsto \boldsymbol{a}$:

$$\delta \boldsymbol{x}(t) = \begin{pmatrix} \cos(\omega_{\rm rf}\, t/2) & -(1/u)\, \sin(\omega_{\rm rf}\, t/2) \\ u \sin(\omega_{\rm rf}\, t/2) & \cos(\omega_{\rm rf}\, t/2) \end{pmatrix} \cdot \boldsymbol{a}(t), \tag{15}$$

where $u = (\omega_1/\omega_2)^{1/2}$ and $\omega_{\rm rf} = 2\pi f_{\rm rf}$. The convenience of the transformation (15) is related to the following circumstance. It provides the analytical solution of the problem (6) when $f_{\rm rf} = 2 f_0$ and when all nonlinear, nonconservative, and rf terms in the equation are neglected. In this special case, the quantity $\boldsymbol{a}$ can be taken as a constant. Due to the smallness of the neglected terms, it is expected that during a time interval of length $T_{\rm rf} = 2\pi/\omega_{\rm rf}$, Eq. (15) with $\boldsymbol{a}(t) = \text{const}$ is a relatively accurate description of the vortex gyration. On the other hand, over time intervals of length equal to many periods $T_{\rm rf}$, the effects of the neglected terms manifest themselves in slow time variations of the variable $\boldsymbol{a}(t)$. This variable $\boldsymbol{a}(t)$ describes the slowly varying amplitude of vortex-core gyrations. Our next goal is to derive an approximate equation governing the dynamics of the slow variable $\boldsymbol{a}(t)$.

By substituting Eq. (15) into Eq. (6) and by taking the time average of the resulting equation over one period of the rf oscillation, one arrives at the following equation:

$$\frac{d\boldsymbol{a}}{dt} = \begin{pmatrix} -d\, \bar{\omega}_0(a) + c_z p_z J_{\rm dc} & -\delta\bar{\omega}_0(a) - J_{\rm rf}\Gamma \\ \delta\bar{\omega}_0(a) - J_{\rm rf}\Gamma & -d\, \bar{\omega}_0(a) + c_z p_z J_{\rm dc} \end{pmatrix} \cdot \boldsymbol{a}, \tag{16}$$

where

$$\bar{\omega}_0(a) = \omega_0 - \nu_{\rm oe} j_{\rm dc} a^2/2 + \Omega_{\rm ms}\{(a/2)^4/[1-(a/2)^2]\} \tag{17}$$

and

$$\delta\bar{\omega}_0(a) = \bar{\omega}_0(a) - \omega_{\rm rf}/2 \tag{18}$$

is the nonlinear detuning parameter. The parameter which controls the coupling with the rf excitations is $\Gamma = \omega_0(q_2 - q_1)/4$. In deriving Eq. (16), use of the fact that $|u-1|$ is a small quantity has been made.

In the condition under study $-d\omega_0 + d c_z p_z < 0$, which in turn implies that no sustained oscillations are excited. In this condition, it is the rf time-varying Oersted field contribution which is responsible for destabilizing the vortex core from its equilibrium position. The stability of small magnetization oscillations around the static equilibrium position can be studied by considering the linearized version of Eq. (16) around $\boldsymbol{a} = 0$. The eigenvalues of such a linearized equation are given by

$$\lambda_{1,2} = -d\,\omega_0 + c_z p_z J_{\rm dc} \pm \sqrt{J_{\rm rf}^2\Gamma^2 - (\omega_0 - \omega_{\rm rf}/2)^2}. \tag{19}$$

The stability is controlled by the sign of the real part of $\lambda_{1,2}$ and the instability boundary in the $(f_{\rm rf}, J_{\rm rf})$ plane is obtained by imposing the vanishing of one eigenvalue. This leads to the equation

$$J_{\rm rf}^2\Gamma^2 - (\omega_0 - \omega_{\rm rf}/2)^2 = (d\,\omega_0 - c_z p_z J_{\rm dc})^2, \tag{20}$$

which describes a hyperbola centered at the point $(\omega_{\rm rf} = 2\omega_0, J_{\rm rf} = 0)$ and with asymptotes along the lines $J_{\rm rf} = \pm(\omega_{\rm rf}/2 - \omega_0)/\Gamma$. In Fig. 3, we show the corresponding phase diagram in the $(f_{\rm rf}, I_{\rm rf})$ plane. When the point $(\omega_{\rm rf}, I_{\rm rf})$ enters the region bounded by the hyperbola (red region in Fig. 3), one of the two eigenvalues (19) becomes positive and $\boldsymbol{a}(t)$ is exponentially growing in time. When the instability sets in, the amplitude of the final regimes depends on the nonlinearities. This will be discussed later on, but we anticipate that after the instability the final nonlinear steady state is periodic with the frequency $f_{\rm rf}/2$. The blue region represents the region of parametric amplification where both eigenvalues are real but still negative.

IV. COMPARISON OF EXPERIMENTS VERSUS ANALYTICAL MODEL

From Eq. (20), one derives that the minimum value of $J_{\rm rf}$ (threshold) such that there exists an interval of $f_{\rm rf}$ in which instability occurs is

$$J_{\rm rf}^{\rm th} = (d\,\omega_0 - c_z p_z J_{\rm dc})/\Gamma. \tag{21}$$

For the particular parameter choices of Fig. 3, i.e., $P = 0.225$, $I_{\rm dc} = 2.5$ mA, $\alpha = 0.01$ [Landau level (LL) damping], $x_0 = 0.3$, and $I_{\rm rf}^{\rm th} = J_{\rm rf}^{\rm th}\pi R^2 = 1$ mA, which is the same value of $I_{\rm rf}^{\rm th}$ observed in the experiments. In the following, we will discuss the cases below (blue dashed line in Fig. 3) and above (black dashed line in Fig. 3) threshold and compare analytical and experimental results.

A. Dynamics below instability threshold

Here we want to analyze the vortex dynamics below $J_{\rm rf}^{\rm th}$. In general, outside the hyperbola the real parts of $\lambda_{1,2}$ are negative and small vortex oscillations are stable. Nevertheless, small vortex oscillations can be driven by thermal fluctuations and the qualitative features of the thermal response can be revealed by considering the linear response of the average amplitude to noise.

The linear equation is the following:

$$\frac{d\boldsymbol{a}}{dt} = \begin{pmatrix} -\Delta_0 & -\delta\omega_0 - J_{\rm rf}\Gamma \\ \delta\omega_0 - J_{\rm rf}\Gamma & -\Delta_0 \end{pmatrix} \cdot \boldsymbol{a}. \tag{22}$$

$\Delta_0 = d\,\omega_0 - c_z p_z J_{\rm dc}$ is the total damping in the linear response, while $\delta\omega_0 = \omega_0 - \omega_{\rm rf}/2$ is the detuning parameter.

At a relatively large detuning, i.e., when $|\delta\omega_0| \gg J_{\rm rf}\Gamma$, the eigenvalues (19) are complex conjugates and are given by $\lambda_{1,2} \approx -\Delta \pm i\,\delta\omega_0$. In this condition, small motion around $\boldsymbol{a} = 0$ consists of damped oscillations with frequency $f_{\rm rf}/2 - f_0$. In terms of frequency response this corresponds to a power spectrum with a peak at the frequency $|f_{\rm rf}/2 - f_0|$ of linewidth $2\Delta_0/(2\pi)$ (bandpass response). By using Eq. (15), i.e., going back to the original variable $\delta\boldsymbol{x}$, and using the fact that the transformation introduces an amplitude modulation of $\delta\boldsymbol{x}$ at frequency $f_{\rm rf}/2$, one can infer that thermally driven vortex dynamics has a power spectral density doubly peaked at f_0 and $f_{\rm rf} - f_0$, with a bandwidth given by Δ_0/π [the

mixing produced by the transformation (15) leads to a signal with frequencies $f_{\rm rf}/2 - f_0 \pm f_{\rm rf}/2 = f_{\rm rf} - f_0, -f_0$ and $f_0 - f_{\rm rf}/2 \pm f_{\rm rf}/2 = f_0, f_0 - f_{\rm rf}$].

The nature of linear relaxation dynamics changes when $\omega_{\rm rf} \approx 2f_0$ (blue region in Fig. 3), i.e., when the eigenvalues become both real and negative. This situation is referred to as *parametric amplification*. The negative sign is a consequence of the condition $\jmath_{\rm rf} < \jmath_{\rm rf}^{\rm th} = \Delta_0/\Gamma$. In particular, when $\jmath_{\rm rf}\Gamma \gg |\delta\omega_0|$, the eigenvalues are given by $\lambda_{1,2} \approx -\Delta_0 \pm \jmath_{\rm rf}\Gamma$. In this situation, the frequency response of $\boldsymbol{a}$ is centered at zero frequency (low pass response) with a bandwidth given by $(\Delta_0 - \jmath_{\rm rf}\Gamma)/\pi$. Thus, by using again Eq. (15), one can conclude that the power spectral density of the thermally driven vortex oscillation for $\jmath_{\rm rf} < \jmath_{\rm rf}^{\rm th}$ and $\jmath_{\rm rf}\Gamma > |\delta\omega_0|$ is centered at $f_{\rm rf}/2$ and has a bandwidth given by $(\Delta_0 - \jmath_{\rm rf}\Gamma)/\pi$ with a good approximation. We observe that in passing from a damped oscillation response to a directed relaxation, the bandwidth is reduced from Δ_0/π to $(\Delta_0 - \jmath_{\rm rf}\Gamma)/\pi$. In addition, the amplitude of the vortex response to an external force increases progressively as $(f_{\rm rf}, \jmath_{\rm rf})$ approaches the instability boundary and theoretically goes to infinity at the boundary. The qualitative features of the parametric amplification (amplitude amplification of noise and reduction of bandwidth) are confirmed by experimental observations, although we do not get a full qualitative agreement. Indeed, by using the values of the parameters associated with the sample under examination, with $I_{\rm rf} = 0.6$ mA we have $\Delta_0/\pi = 600$ kHz and $(\Delta_0 - \jmath_{\rm rf}\Gamma)/\pi = 224$ kHz. If we compare with the measurements of the parametric amplification regime reported in Fig. 2(b), we observe that the linewidth of the response is estimated to be approximately 2.1 MHz, which is one order of magnitude larger than the theoretically predicted one. These discrepancies are related to the simplistic model used to describe thermal fluctuations. A more accurate analysis should take into account elementary excitations around the vortex ground state. A detailed analysis of this issue and of the thermal response of the MTJ vortex-based system is beyond the scope of this paper.

B. Dynamics above instability threshold

Inside the instability region (red region in Fig. 3), the equilibrium position $\boldsymbol{x}_0$ becomes unstable and the study of the system response requires the inclusion of nonlinear terms. This has been done in Fig. 4(a), which is a generalization of Fig. 3. The nonlinear regime after instability can be found by searching for nonzero equilibria of the general equation (16) which, by taking into account Eq. (15), correspond to the steady state of the vortex at a frequency $f_{\rm rf}/2$. Equation (16) always admits the solution $\boldsymbol{a} = 0$, which corresponds to the equilibrium position $\boldsymbol{x}_0$. Due to the structure of Eq. (16), the nonlinearly saturated steady state can be conveniently found by imposing that the determinant of the matrix at the RHS of Eq. (16) is zero, which leads to the equation

$$\jmath_{\rm rf}^2\Gamma^2 - [\bar{\omega}_0(a) - \omega_{\rm rf}/2]^2 = [d\,\bar{\omega}_0(a) - c_z p_z \jmath_{\rm dc}]^2 . \quad (23)$$

The nonlinear response of the system can be then obtained by keeping $\jmath_{\rm rf}$ fixed and interpreting Eq. (23) as an implicit relation between a and $\omega_{\rm rf}$. The result of this analytical computation for the particular case of $I_{\rm rf} = 1.8$ mA [dashed black line in Fig. 4(a)] is shown in Fig. 4(b). Solid lines indicate stable regimes, while the dashed lines indicate unstable regimes. In the white region only one state exists and it is stable ($\boldsymbol{a} = 0$). In the red region, parametric excitation takes place and the amplitude of $\boldsymbol{a}$ starts to increase while the state at $\boldsymbol{a} = 0$ becomes unstable. In the region of coexistence (green region in Fig. 4) the stable large amplitude regime coexists with the stable equilibrium position of the vortex. This is due to the fact that the large amplitude regime exists in a range of frequency which goes well outside the region of linear instability of the equilibrium position of the vortex. In fact, this type of coexistence is typical of the nonlinear parametrically driven response of an oscillator.[2] The coexistence of two stable regimes leads to the prediction of a hysteresis behavior of the amplitude of oscillation under an alternate variation of the frequency. This hysteresis phenomenon might be masked in the presence of thermal fluctuations and hopping between the two stable regimes.

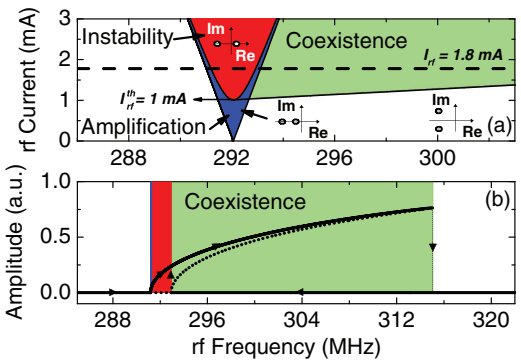

FIG. 4. (Color online) (a) Phase diagram in the $(f_{\rm rf}, \jmath_{\rm rf})$ plane with indications of the region of parametric instability (red), coexistence of stable regimes (green), and parametric amplification (blue). (b) Analytically computed amplitude response vs $f_{\rm rf}$, according to Eq. (23) with $I_{\rm rf} = 1.8$ mA, which corresponds to a power value of -11 dBm. The values of the parameters used are $P = 0.225$, $I_{\rm dc} = 2.5$ mA, $\alpha = 0.01$ (LL damping), and $x_0 = 0.3$.

To verify the prediction of the *coexistence* (green region in Fig. 4), we present in Fig. 5 a series of measurements performed on another junction from the same wafer, in which the vortex gyrotropic dynamics has a few MHz difference for the thermal resonant frequency. The measurements have been performed with $H_{\rm perp} = 4.48$ kG, $I_{\rm dc} = 2.5$ mA, and $I_{\rm rf} = 1.8$ mA (rms value) corresponding to -11 dBm of rf power.

In Figs. 5(a) and 5(b), we plot the vortex frequency f and the power of the emitted signal as a function of $f_{\rm rf}$, respectively. At low frequencies ($f_{\rm rf} < 275$ MHz), we detect only a small peak around f_0 corresponding to the thermally excited signal. At $f_{\rm rf} = 275$ MHz, a second peak with a very small power [note the logarithmic scale in Fig. 5(b)] centered at $f_{\rm rf} - f_0$ appears. This situation with two small peaks, whose power increases with $f_{\rm rf}$, lasts until 285 MHz. A typical spectrum in this regime is shown in Fig. 5(c). Between 275 and 285 MHz the power for both signals increases, as predicted by the theory. This is a sign of *parametric amplification*, i.e., blue region in Fig. 4. In the same interval both signals approach the $f_{\rm rf}/2$ frequency. From $f_{\rm rf} = 285$ to 305 MHz, the spectra contain a main peak with large power and two sidebands. The analysis of these thermally

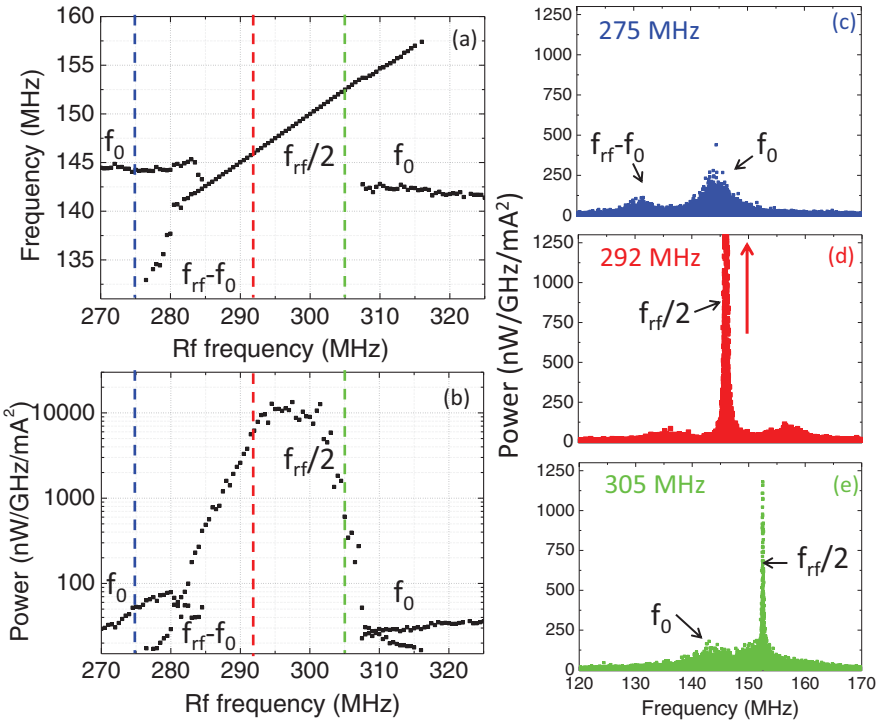

FIG. 5. (Color online) (a) Vortex frequency f vs rf frequency f_{rf}. (b) Power density vs rf frequency f_{rf}. All values are the result of a Lorentzian fit applied to the raw spectra in the same manner of Fig. 2. (c)–(e) Power density vs frequency f for three values of f_{rf}: 275, 295, and 305 MHz. Note that these measurements have been made with an out-of-plane field $H_{perp} = 4.48$ kG, a subcritical dc current $I_{dc} = 2.5$ mA, and a rf current $I_{rf} = 1.8$ mA, corresponding to a power of -11 dBm.

excited sideband signals[40] in the parametric regime is out of the scope of this paper and for the sake of clarity we have not reported their values in Figs. 5(a) and 5(b). In this rf frequency range, the vortex frequency is locked to the source signal, i.e., $f_{rf}/2$, and thus evolves linearly with the rf frequency [see Fig. 5(a)]. As shown in Fig. 5(b), the peak power increases exponentially to reach a maximum of $\approx 10\ \mu$W/GHz/mA^2 at $f_{rf} = 295$ MHz. The linewidth obtained at this rf frequency is only a few tens of kHz. Then, between 295 and 300 MHz, the power spectral density stagnates, meaning that the amplitude of the vortex oscillation saturates. Further increasing f_{rf} above 300 MHz, the power density starts to decline. Moreover, at $f_{rf} = 305$ MHz, we detect again a second peak centered at f_0 [see Fig. 5(e)].

As expected by the analytical calculations [see Fig. 4(b)], the two peaks, one at $f_{rf}/2$ and one at f_0, detected in the region between 305 and 315 MHz, correspond to the two states predicted in the region of coexistence. Notably, the main features of the power density evolution [see Fig. 5(b)] are in agreement with the evolution expected by the theory [see Fig. 4(b)]: The oscillation amplitude grows monotonically from 10^2 to 10^4 nW/GHz/mA^2 between 282 and 295 MHz. Conversely, we find that the opposite reduction of power occurs very sharply in few MHz (from 300 to 305 MHz). This behavior corresponds to the soft-hard regime discrimination already observed for the case of uniform magnetization.[35] Note that thermal effects, which are not considered in the model, result in a blur of the transition between the different regimes, and consequently allow some thermally induced transitions from one state to the other. Furthermore, we believe that another impact of thermal energy is to avoid the experimental observation of the hysteresis effect predicted by the analytical model [see Fig. 4(b)]. Complementary experiments at low temperature and an analysis of the parametrically driven vortex dynamics in the time domain might be helpful to address more precisely the impact of temperature on the nonlinear vortex dynamics.

V. CONCLUSIONS

In summary, we have presented a comprehensive investigation of parametric excitation of vortex dynamics in a MTJ-based spin-transfer oscillator. Moreover, we propose an analytical model to predict the phase diagram of our vortex system in the presence of an external rf current at about twice the natural vortex frequency. We report an observation in spin-torque devices of the different parametric regimes of amplification and instability. Finally, we demonstrate, both experimentally and theoretically, the coexistence of two parametric states of the vortex dynamics, evidencing the important role of nonlinearities. The parametric excitation in vortex-based devices might be used for highly efficient rf detection or low-noise amplification using the specific potential of these devices in tuning their rf features through both the rf and dc current.

ACKNOWLEDGMENTS

The authors acknowledge N. Locatelli and N. Reyren for fruitful discussion, Y. Nagamine, H. Maehara, and K. Tsunekawa of CANON ANELVA for preparing the MTJ films, and financial support from the ANR agency (SPINNOVA ANR-11-NANO-0016) and a EU FP7 Grant (MOSAIC No. ICT-FP7-n.317950). E.G. acknowledges DGA-CNES for financial support. C.S. acknowledges financial support from MIUR-PRIN 2010-11 Project2010ECA8P3 “DyNanoMag.”

APPENDIX A: DESCRIPTION OF THE THIELE EQUATION

The Thiele-like equation[29,33] describing the magnetization dynamics is written as

$$-\boldsymbol{G}\times\frac{d\boldsymbol{X}}{dt}+\widehat{D}\cdot\frac{d\boldsymbol{X}}{dt}=-\frac{\partial W}{\partial \boldsymbol{X}}+\boldsymbol{F}_{\rm st}+\boldsymbol{F}_{\rm eff}, \quad \text{(A1)}$$

where $\boldsymbol{X}=X_1\boldsymbol{e}_x+X_2\boldsymbol{e}_y$ and $(\boldsymbol{e}_x,\boldsymbol{e}_y)$ are the unit vectors of a Cartesian reference frame in the plane of the disk. The variable $\boldsymbol{X}$ is understood to fulfill the condition $|\boldsymbol{X}|\leqslant R$, where R is the radius of the pillar.

The first term on the left-hand side (LHS) of Eq. (A1) is the gyroforce which is defined through the gyrovector[32]

$$\boldsymbol{G}=-\boldsymbol{e}_z 2\pi pLM_s/\gamma, \quad \text{(A2)}$$

where L is the layer thickness, M_s the free layer saturation magnetization, and $\gamma=1.76\times10^{11}$ rad s^{-1} T^{-1} is the gyromagnetic ratio. The vector $\boldsymbol{e}_z$ is the unit vector of the axis z which is the axis of symmetry of the MTJ pillar and it is directed from the fixed layer to the free layer. The constant p is the polarity of the vortex (sign of the out-of-plane component of magnetization in the vortex core) which is taken to be $p=+1$.

The second term on the LHS of Eq. (A1) is the viscous-type damping, and the quantity $\hat{D}(\boldsymbol{X})$ is a positive definite symmetric tensor.[32] Due to the rotationally invariant geometry of the system, we assume that $\hat{D}(\boldsymbol{X})=D(X)\mathcal{I}$, where $\mathcal{I}$ is the identity matrix and $X=|\boldsymbol{X}|$. Since the dependence of $D(X)$ on X is not very strong, for the sake of simplicity, we assume that damping is independent of $\boldsymbol{X}$ and it has the expression

$$D(X)=D=\alpha\eta|\boldsymbol{G}|, \quad \text{(A3)}$$

where η is a geometrical factor given by the expression[31] $\eta=(1/2)\ln(R/2b)-1/8$, and b is the vortex-core radius, which we assume to be $b=2l_{\rm ex}$, where $l_{\rm ex}$ is the exchange constant (the typical value of this quantity is $l_{\rm ex}\approx6.0$ nm).

The first term on the right-hand side (RHS) of Eq. (A1) is the force associated with the gradient of the vortex energy $W(\boldsymbol{X})$. This force, along with the gyroforce, are usually the dominant terms in the equation. The vortex energy is the sum of two terms $W(\boldsymbol{X})=W_{\rm ms}(\boldsymbol{X})+W_{\rm oe}(\boldsymbol{X})$, which are, respectively, the vortex magnetostatic energy and the vortex energy due to the Oersted field generated by the current injected in the pillar. In cylindrical pillars perpendicularly traversed by a spatially uniform current density, the vortex energy depends only on the amplitude X of the displacement and not on its direction. The expressions of the above two contributions to the vortex energy are

$$W_{\rm ms}(X)=-(\kappa_{\rm ms}R^2/2)\log[1-(X/2R)^2], \quad \text{(A4)}$$

$$W_{\rm oe}(X)=\jmath\left(\tfrac{1}{2}\lambda_{\rm oe}X^2+\tfrac{1}{4}\lambda'_{\rm oe}X^4/R^2\right). \quad \text{(A5)}$$

The expression of magnetostatic energy (A4) has been derived by Gaididei,[34] and the parameter $\kappa_{\rm ms}$ is given by the formula $\kappa_{\rm ms}=(10/9)\mu_0M_s^2L^2/R$. The Taylor expansion of $W_{\rm ms}(X)$ up to fourth order power in X agrees with the expression normally used to analyze the vortex-core oscillation of moderate amplitude.[31,32] On the other hand, formula (A4) is expected to be more accurate for large vortex-core motion, when the vortex core is relatively close to the boundary of the disk.[34] The nonlinear nature of vortex dynamics is mainly due to the terms in $W(X)$ which are of order larger than X^2.

The Oersted energy (A5) is responsible for the direct coupling of vortex dynamics with rf excitations as it is proportional to the injected current density:

$$\jmath=I/(\pi R^2)=\jmath_{\rm rf}\cos(2\pi f_{\rm rf}t)+\jmath_{\rm dc}, \quad \text{(A6)}$$

with $\jmath_{\rm rf}=I_{\rm rf}/(\pi R^2)$ and $\jmath_{\rm dc}=I_{\rm dc}/(\pi R^2)$. The other parameters in Eq. (A5) are given by the following expressions:[31] $\lambda_{\rm oe}=0.85\mu_0M_sRL$ and $\lambda'_{\rm oe}=-0.5\lambda_{\rm oe}$.

The second term on the RHS of Eq. (A1) is the component of the spin-transfer related forces which is responsible for compensating the damping of vortex dynamics. It has been singled out from the other terms because of its special character of being a negative damping term. Its expression is given by

$$\boldsymbol{F}_{{\rm st},z}=C_zp_z\jmath\,\boldsymbol{e}_z\times\boldsymbol{X}, \quad \text{(A7)}$$

where $p_z=\boldsymbol{p}\cdot\boldsymbol{e}_z$ is the perpendicular component of the polarizer magnetization, $C_z=|\boldsymbol{G}|\gamma\sigma/2$, a constant measuring the spin-torque efficiency, and $\sigma=\hbar P/(2|e|LM_s)$; P is the spin polarization, $\hbar$ the Planck constant, and e the electron charge.

The term $\boldsymbol{F}_{\rm eff}$ on the RHS of Eq. (A1) takes into account all additional forces acting on the vortex and it is the sum of three terms: $\boldsymbol{F}_{\rm eff}=\boldsymbol{F}_{\rm ext}+\boldsymbol{F}_{{\rm st},xy}+\boldsymbol{F}_{\rm def}$. The first term takes into account the effects of the in-plane external $\boldsymbol{H}_{{\rm ext},xy}$ magnetic field to which the free layer is subject. This field is assumed to take also into account the stray field coupling between the free layer and the SAF polarizer. The term $\boldsymbol{F}_{{\rm st},xy}$ is due to the spin-torque forces produced by the in-plane component $\boldsymbol{p}_{xy}$ of the polarizer magnetization.[31] The term $\boldsymbol{F}_{\rm def}$ takes into account extra forces such as those due to defects.[41,42] The terms above are taken as constant with respect to $\boldsymbol{X}$ in the present analysis. The form of $\boldsymbol{F}_{{\rm st},xy}$ has been derived in the literature,[31] but its exact expression is not crucial as the $\boldsymbol{F}_{\rm eff}$ is estimated through measurements. Thus, for the purpose of our analysis, it is sufficient to write $\boldsymbol{F}_{\rm eff}$ as follows:

$$\boldsymbol{F}_{\rm eff}=C\tfrac{2}{3}\pi M_sLR(\boldsymbol{e}_z\times\boldsymbol{H}_{{\rm eff},xy}), \quad \text{(A8)}$$

where C is the vortex chirality which is assumed to be $+1$ in the following. In general, expression (A8) is used to describe the force on the vortex due to the external field. The use of $\boldsymbol{H}_{{\rm eff},xy}$ enables us to takes into account the contribution of the term $\boldsymbol{F}_{{\rm st},xy}$ and $\boldsymbol{F}_{\rm def}$.

The main effect of $\boldsymbol{F}_{\rm eff}$ under dc excitation is to produce a break of the rotational symmetry of the system which leads to a static shift of the core position from the MTJ center to the position $\boldsymbol{X}_0$. The effect of this force is indeed equivalent to an effective in-plane field $\boldsymbol{H}_{{\rm eff},xy}$. Even if the precise determination of $\boldsymbol{H}_{{\rm eff},xy}$ is not easy to obtain, from resistance versus in-plane field measurements, we estimate it to be a few tens of Gauss, thus enough to break the system symmetry even at low injected rf currents.

In addition, it is important to discuss briefly the role of the strong out-of-plane external field $H_{{\rm ext},z}$ to which the MTJ structure is subject. This field is instrumental in tilting the magnetization of the polarizer in order to increase the efficiency of the spin-torque term. The tilting of the orientation of magnetization in the polarizer can be approximately obtained by the formula $p_z\approx H_{{\rm ext},z}/M_s^{\rm saf}$, where $M_s^{\rm saf}$ is the saturation

magnetization of the polarizer. Due to $H_{\mathrm{ext},z}$, the curling part of the magnetic vortex (the one outside the vortex core) is tilted out of plane, leading to an out-of-plane component of magnetization

$$m_z = \cos\Theta \approx H_{\mathrm{ext},z}/M_s = h_z, \tag{A9}$$

where Θ is the angle between magnetization and the z axis. This tilting leads to a change of the parameters entering in the energy of the vortex as follows: $\kappa_{\mathrm{ms}}(h_z) = \kappa_{\mathrm{ms}}(0)(1-h_z^2)$, $\lambda_{\mathrm{oe}}(h_z) = \lambda_{\mathrm{oe}}(0)(1-h_z^2)^{1/2}$, where $\kappa_{\mathrm{ms}}(0)$ and $\lambda_{\mathrm{oe}}(0)$ are the values of the parameters previously specified. The fact that magnetization goes out of plane also affects the gyrovector, $G(h_z) = G(0)(1-h_z)$, where $G(0)$ is the value of $|\boldsymbol{G}|$ given by Eq. (A2). Other important parameters affected by $H_{\mathrm{ext},z}$ are those related to nonconservative effects: damping and spin-torque terms. For these terms we have the following rescaling: $\boldsymbol{F}_{\mathrm{st},z}(\boldsymbol{X}) = C_z J p_z(h_z)(1-h_z^2)\boldsymbol{e}_z \times \boldsymbol{X}$ and $D = G(0)\alpha\eta(h_z)(1-h_z^2)$. The change of η as a function of h_z is ascribed to the change of the vortex radius in functions of h_z which, for the junctions under study, is approximated by an exponential function $b(h_z) = b(0)e^{1.19h_z}$.[31] In summary, as we have discussed above, the presence of strong $H_{\mathrm{ext},z}$ is taken into account by an appropriate rescaling[12,31] of the parameters entering in all terms of Eq. (A1).

APPENDIX B: NORMALIZED EQUATION

In order to simplify the analysis, we proceed to a normalization of Eq. (A1). By dividing both sides of the equation by $|G(h_z)|R$, one obtains the following normalized equation:

$$\boldsymbol{e}_z \times \frac{d\boldsymbol{x}}{dt} + d\frac{d\boldsymbol{x}}{dt} = -\Omega(x,J)\boldsymbol{x} + c_z p_{zJ}\,\boldsymbol{e}_z \times \boldsymbol{x} + \boldsymbol{f}, \tag{B1}$$

where $\boldsymbol{x} = \boldsymbol{X}/R$ is the vortex displacement measured in units of R,

$$d = D(h_z)/|G(h_z)| = \alpha\eta(h_z)(1+h_z) \tag{B2}$$

is the normalized damping constant, and

$$\boldsymbol{f} = \boldsymbol{F}_{\mathrm{eff}}/(|G(h_z)|R) \tag{B3}$$

takes into account all in-plane constant forces acting on the vortex.

In Eq. (B1) we have neglected the dependence of the various parameters on h_z for notational simplicity. The constant c_z in the second term on the RHS of Eq. (B1) is given by

$$c_z = \frac{\pi M_s L\sigma}{|G(h_z)|} = \frac{\gamma\sigma}{2}(1+h_z). \tag{B4}$$

The function $\Omega(x,J)$ is the frequency of the vortex free gyrotropic oscillation, as a function of the displacement and the injected current, and it is related to the vortex energy by means of the following equation:

$$\Omega(x,J) = \frac{1}{|G(h_z)|}\frac{1}{X}\frac{\partial W}{\partial X}\bigg|_{X=xR}. \tag{B5}$$

By substituting formulas (A4) and (A5) into Eq. (B5), one obtains

$$\Omega(x,J) = \Omega_{\mathrm{ms}}\left(\frac{1}{1-(x/2)^2}\right) + J\nu_{oe}\left(1-\frac{x^2}{2}\right), \tag{B6}$$

where

$$\Omega_{\mathrm{ms}} = \frac{\kappa_{\mathrm{ms}}(h_z)}{|G(h_z)|} = \frac{5}{9\pi}\gamma\mu_0 M_s\frac{L}{R}(1+h_z) \tag{B7}$$

and

$$\nu_{\mathrm{oe}} = \frac{\lambda_{\mathrm{oe}}(h_z)}{|G(h_z)|} = \frac{0.85}{2\pi}\gamma\mu_0 R\sqrt{\frac{1+h_z}{1-h_z}}. \tag{B8}$$

To make Eq. (B1) explicit with respect to $d\boldsymbol{x}/dt$, we take the vector product of both sides of the equation with $\boldsymbol{e}_z$ and then, by taking into account that

$$\frac{d\boldsymbol{x}}{dt} - d\boldsymbol{e}_z \times \frac{d\boldsymbol{x}}{dt} = \begin{pmatrix} 1 & d \\ -d & 1 \end{pmatrix}\cdot\frac{d\boldsymbol{x}}{dt}, \tag{B9}$$

we can write Eq. (B1) in the explicit form

$$\frac{d\boldsymbol{x}}{dt} = \begin{pmatrix} 1 & d \\ -d & 1 \end{pmatrix}^{-1}\cdot\left[\Omega(x,J)\boldsymbol{e}_z \times \boldsymbol{x} + c_z p_{zJ}\,\boldsymbol{x} + \boldsymbol{v}\right], \tag{B10}$$

where

$$\boldsymbol{v} = -\boldsymbol{e}_z \times \boldsymbol{f}. \tag{B11}$$

Finally, by taking into account that in the usual condition d, $c_z p_{zJ}$, and $\boldsymbol{v}$ are small quantities, and neglecting all terms which contains second or higher order products of these quantities, we obtain Eq. (1).

*Corresponding author: paolo.bortolotti@thalesgroup.com
†Present address: ETH Zurich, 101 Rämistrasse, 8092 Zurich, Switzerland.

[1] M. Faraday, Philos. Trans. R. Soc. London **121**, 299 (1831).
[2] L. D. Landau and E. M. Lifshitz, *Mechanics* (Pergamon, Oxford, UK, 1976), Sec. 29.
[3] V. I. Arnold, *Mathematical Methods of Classical Mechanics* (Springer, New York, 1989), Chap. 5, Sec. 25.
[4] *Parametric Resonance in Dynamical Systems*, edited by T. I. Fossen and H. Nijmeijer (Springer, New York, 2012).
[5] D. Rugar and P. Grutter, Phys. Rev. Lett. **67**, 699 (1991).
[6] G. Prakash, A. Raman, J. Rhoads, and R. G. Reinfenberger, Rev. Sci. Instrum. **83**, 065109 (2012).
[7] J. M. Manley and H. E. Rowe, Proc. IRE **44**, 904 (1956); **46**, 850 (1958).
[8] W. Lee and E. Afshari, IEEE Trans. Circuits Syst., I **58**, 479 (2011).
[9] V. S. Lvov, *Wave Turbulence Under Parametric Excitation* (Springer, New York, 1994).
[10] H. Suhl, Proc. IRE **44**, 1270 (1956).
[11] E. Schlömann, J. Appl. Phys. **33**, 527 (1962).
[12] B. A. Ivanov and G. M. Wysin, Phys. Rev. B **65**, 134434 (2002).

[13]A. Slavin and V. S. Tiberkevich, IEEE Trans. Magn. **45**, 1875 (2008).
[14]D. C. Ralph and M. D. Stiles, J. Magn. Magn. Mater. **320**, 1190 (2008).
[15]P. Villard, U. Ebels, D. Houssameddine, J. Katine, D. Mauri, B. Delaet, P. Vincent, M. C. Cyrille, B. Viala, J. P. Michel, J. Prouvee, and F. Badets, IEEE J. Solid-State Circuits **45**, 214 (2010).
[16]S. I. Kiselev, J. C. Sankey, I. N. Krivorotov, N. C. Emley, R. J. Schoelkopf, R. A. Buhrman, and D. C. Ralph, Nature (London) **425**, 380 (2003).
[17]W. H. Rippard, M. R. Pufall, S. Kaka, T. J. Silva, and S. E. Russek, Phys. Rev. B **70**, 100406 (2004).
[18]J. C. Sankey, P. M. Braganca, A. G. F. Garcia, I. N. Krivorotov, R. A. Buhrman, and D. C. Ralph, Phys. Rev. Lett. **96**, 227601 (2006).
[19]V. S. Pribiag, I. N. Krivorotov, G. D. Fuchs, P. M. Braganca, O. Ozatay, J. C. Sankey, D. C. Ralph, and R. A. Buhrman, Nat. Phys. **3**, 498 (2007).
[20]M. R. Pufall, W. H. Rippard, M. L. Schneider, and S. E. Russek, Phys. Rev. B **75**, 140404(R) (2007).
[21]Q. Mistral, M. van Kampen, G. Hrkac, J.-V. Kim, T. Devolder, P. Crozat, C. Chappert, L. Lagae, and T. Schrefl, Phys. Rev. Lett. **100**, 257201 (2008).
[22]I. N. Krivorotov, N. C. Emley, R. A. Buhrman, and D. C. Ralph, Phys. Rev. B **77**, 054440 (2008).
[23]B. Georges, J. Grollier, V. Cros, A. Fert, A. Fukushima, H. Kubota, K. Yakushijin, S. Yuasa, and K. Ando, Phys. Rev. B **80**, 060404 (R) (2009).
[24]B. Georges, J. Grollier, M. Darques, V. Cros, C. Deranlot, B. Marcilhac, G. Faini, and A. Fert, Phys. Rev. Lett. **101**, 017201 (2008).
[25]M. Quinsat, D. Gusakova, J. F. Sierra, J. P. Michel, D. Houssameddine, B. Delaet, M.-C. Cyrille, U. Ebels, B. Dieny, L. D. Buda-Prejbeanu, J. A. Katine, D. Mauri, A. Zeltser, M. Prigent, J.-C. Nallatamby, and R. Sommet, Appl. Phys. Lett. **97**, 182507 (2010).
[26]M. W. Keller, M. R. Pufall, W. H. Rippard, and T. J. Silva, Phys. Rev. B **82**, 054416 (2010).
[27]Y. Pogoryelov, P. K. Muduli, S. Bonetti, F. Mancoff, and J. Kerman, Appl. Phys. Lett. **98**, 192506 (2011).
[28]D. Gusakova, M. Quinsat, J. F. Sierra, U. Ebels, B. Dieny, L. D. Buda-Prejbeanu, M.-C. Cyrille, V. Tiberkevich, and A. N. Slavin, Appl. Phys. Lett. **99**, 052501 (2011).
[29]A. Dussaux, B. Georges, J. Grollier, V. Cros, A. V. Khvalkovskiy, A. Fukushima, M. Konoto, H. Kubota, K. Yakushiji, S. Yuasa, K. A. Zvezdin, K. Ando, and A. Fert, Nat. Commun. **1**, 1 (2010).
[30]A. V. Khvalkovskiy, J. Grollier, A. Dussaux, K. A. Zvezdin, and V. Cros, Phys. Rev. B **80**, 140401(R) (2009).
[31]A. Dussaux, A. V. Khvalkovskiy, P. Bortolotti, J. Grollier, V. Cros, and A. Fert, Phys. Rev. B **86**, 014402 (2012).
[32]K. Y. Guslienko, B. A. Ivanov, V. Novosad, Y. Otani, H. Shima, and K. Fukamichi, J. Appl. Phys. **91**, 8037 (2002).
[33]K. Y. Guslienko, J. Nanosci. Nanotechnol. **8**, 2745 (2008).
[34]Y. Gaididei, V. P. Kravchuk, and D. D. Sheka, Int. J. Quantum Chem. **110**, 83 (2010).
[35]S. Urazhdin, V. Tiberkevich, and A. Slavin, Phys. Rev. Lett. **105**, 237204 (2010).
[36]S. Y. Martin, N. de Mestier, C. Thirion, C. Hoarau, Y. Conraux, C. Baraduc, and B. Dieny, Phys. Rev. B **84**, 144434 (2011).
[37]A. Dussaux, A. V. Khvalkovskiy, J. Grollier, V. Cros, A. Fukushima, M. Konoto, H. Kubota, K. Yakushiji, S. Yuasa, K. Ando, and A. Fert, Appl. Phys. Lett. **98**, 132506 (2011).
[38]P. Bortolotti, A. Dussaux, J. Grollier, V. Cros, A. Fukushima, H. Kubota, K. Yakushiji, S. Yuasa, K. Ando, and A. Fert, Appl. Phys. Lett. **100**, 042408 (2012).
[39]S. Petit, C. Baraduc, C. Thirion, U. Ebels, Y. Liu, M. Li, P. Wang, and B. Dieny, Phys. Rev. Lett. **98**, 077203 (2007).
[40]M. d'Aquino, C. Serpico, R. Bonin, G. Bertotti, and I. D. Mayergoyz, Phys. Rev. B **82**, 064415 (2010).
[41]J. Tobik, V. Cambel, and G. Karapetrov, Phys. Rev. B **86**, 134433 (2012).
[42]J.-S. Kim, O. Boulle, S. Verstoep, L. Heyne, J. Rhensius, M. Klaui, L. J. Heyderman, F. Kronast, R. Mattheis, C. Ulysse, and G. Faini, Phys. Rev. B **82**, 104427 (2010).